arXiv:mtrl-th/9602001v1 7 Feb 1996

The Structure, Dynamics and Electronic Structure of Liquid Ag-Se Alloys Investigated by Ab Initio Simulation

F. Kirchhoff, J. M. Holender and M. J. Gillan
Physics Department, Keele University
Keele, Staffordshire ST5 5BG, U.K.

(February 8, 2008)

Ab initio molecular-dynamics simulations have been used to investigate the structure, dynamics and electronic properties of the liquid alloy $Ag_{1-x}Se_x$ at 1350 K and at the three compositions $x = 0.33$, 0.42 and 0.65. To provide a point of reference, calculations are also presented for the equilibrium structure and the electronic structure of the α-Ag_2Se crystal. The calculations are based on density-functional theory in the local density approximation and on the pseudopotential plane-wave method. For the solid, we find excellent agreement with experiment for the equilibrium lattice parameters and the atomic coordinates of the 12-atom orthorhombic unit cell, and we present an analysis of the electronic density of states and density distribution. The reliability of the liquid simulations is confirmed by detailed comparisons with very recent neutron diffraction results for the partial structure factors and radial distribution functions (RDF) of the stoichiometric liquid Ag_2Se. Comparison with the predictions of an empirical interaction model due to Rino *et al.* is also given for ℓ-Ag_2Se. The *ab initio* simulations show a dramatic change of the Se-Se RDF with increasing Se content. This change is due to the formation of Se clusters bound by covalent bonds, the Se-Se bond length being almost the same as in pure *c*-Se and ℓ-Se. The clusters are predominantly chain-like, but for higher x there is a significant fraction of 3-fold coordinated Se atoms. It is shown that the equilibrium fractions of Se present as isolated atoms and in clusters can be understood on a simple charge-balance model based on an ionic interpretation. The Ag diffusion coefficient in the simulated stoichiometric liquid is consistent with experimental values measured in the high-temperature superionic solid. The Ag and Se diffusion coefficients both increase with Se content, in spite of the Se clustering. An analysis of the Se-Se bond dynamics reveals surprisingly short bond lifetimes of less than 1 ps. The electronic density of states (DOS) for ℓ-Ag_2Se strongly resembles that of the solid. Some of the changes of DOS with composition arise directly from the formation of Se-Se covalent bonds. Results for the electronic conductivity σ obtained using the Kubo-Greenwood approximation are in adequate agreement with experiment for ℓ-Ag_2Se, but for the high Se contents the simulation results for σ are 3–4 times greater than experimental values. Possible reasons for this are discussed.

I. INTRODUCTION

The study of liquid binary alloys has been an extremely fruitful source of insights into the relations between structure and electronic properties in condensed matter. There has been a vast amount of experimental work on metallic and semiconducting binary liquids, and it has been well known for many years that their properties often vary dramatically with composition[1,2]. Famous cases are the Cs-Au and Mg-Bi alloys[3,4], in which the pure elements are good metals, but nevertheless the stoichiometric mixtures (CsAu and Mg_3Bi_2) have very low conductivities, and their structures are characteristic of molten salts. These effects arise from the electronegativity difference between the elements, and the resulting charge transfer, partial ionicity and heterocoordination. In systems where one of the elements is a semiconductor in the liquid state – for example alloys of metals with S or Se – even richer behavior can be expected, since variation of composition should change the bonding from metallic through partially ionic to covalent. We report here a set of simulations of the liquid Ag-Se system performed using *ab initio* molecular dynamics (AIMD), which we have used to explore these effects.

The electrical conductivity σ of the $Ag_{1-x}Se_x$ system has been measured over most of the composition range at temperatures from 973 to 1573 K[5–8]. As the composition goes from pure ℓ-Ag to the stoichiometric alloy Ag_2Se, σ decreases from the typically metallic value of $\sim 50000\ \Omega^{-1}\text{cm}^{-1}$ to typical semiconducting values of $\sim 500\ \Omega^{-1}\text{cm}^{-1}$. This strongly suggests the formation of a pseudogap in the electronic density of states at the stoichiometric composition, with the Fermi energy lying in this gap. As the Se content is further increased, σ varies rather little over the range between $x = 0.33$ and $x = 0.65$, and then descends to very low values of $\sim 1\ \Omega^{-1}\text{cm}^{-1}$ at 700 K as the Ag content goes to zero[9]. The properties of pure ℓ-Se have been very extensively studied[10], and it is known to have a gap of *ca.* 1.9 eV in the density of states just above its melting point (∼490 K), so that it is a wide-gap semiconductor. This gap decreases with increasing temperature, and appears to be *ca.* 0.7 eV at 1350 K and 100 bar[11].

Pure ℓ-Ag has the rather closed-packed structure and high coordination number (*ca.* 12) expected from its f.c.c. crystal structure[12]. Until very recently, the structure of ℓ-Ag_2Se had been measured only at the level of the neutron-weighted structure factor[13], but neutron diffraction combined with isotope variation has now been used to measure the partial structure factors and hence the partial radial distribution functions[14]. These reveal the heterocoordination characteristic of ionic or partially ionic liquids, as will be discussed more fully below. Diffraction studies on ℓ-Se have been made by several independent groups[15–17], and it is well established that the average coordination of the atoms is close to 2.0 over a wide range of temperatures and pressures from the melting point up to 1773 K and 815 bar. It is widely believed that this coordination indicates the presence of extended chain-like structures, and there is support for this from simulation work[18,19]. These facts imply that there must be major changes of atomic ordering as the composition is varied from pure ℓ-Ag to pure ℓ-Se. However, nothing is yet known about the structure of the alloys except at the stoichiometric composition.

The aim of the work reported here is to use *ab initio* molecular dynamics simulation (AIMD)[20,21] to investigate the structure, the atomic dynamics and the electronic structure of the liquid Ag-Se alloys at different compositions. The issues we want to address are: the relationship between the electronic structure of the liquid and the solid; the characteristics of the electronic density of states and electron distribution as a function of composition; the variation of liquid structure with composition, and particularly how the apparently ionic structure of ℓ-Ag-Se goes over to the chain-like structure of ℓ-Se; and the way this liquid structure is related to the dynamics of the ions. At present, there is almost no experimental information about any of these questions. Of course, before we address any of these issues, we have to show that our AIMD techniques are able to give a faithful representation of the real material. Because of this, we will begin by presenting calculations on the α-Ag_2Se crystal, which has a rather complex structure and gives a good test of our methods. Our study of the crystal also provides an essential reference point for discussing the properties of the liquid.

AIMD is ideally suited to this type of problem. The energetics of the system and the forces on the ions are calculated by first-principles quantum methods, with no adjustable parameters, and without the need for the empirical interionic potentials used in earlier simulations on many liquid mixtures, including ℓ-Ag_2Se[22]. In addition, the thermal-equilibrium structure, atomic dynamics and electronic structure are all calculated together in a completely unified and self-consistent way. AIMD techniques have been used to investigate a number of other liquid metals and semiconductors, including the binary alloys K-Si[23], Na-Sn[24], Cs-Pb[25] and Ga-Se[26]. Preliminary results of the work presented here have already been published elsewhere[27]. The rest of the paper is organised as follows. In Sec. II, we summarize the simulation techniques, and we then present in Sec. III our calculations on the equilibrium structure and the electronic structure of α-Ag_2Se. Our simulation results on the liquid Ag-Se alloys are reported in Sec. IV, where we examine successively the structure, the atomic dynamics and the electronic properties, including the density of states and the electronic conductivity. We present a brief, discussion of the relation between atomic ordering and electronic properties in Sec. V, and our conclusions are summarized in Sec. VI.

II. COMPUTATIONAL METHODS

Our *ab initio* molecular dynamics (AIMD) technique is closely related to the Car-Parrinello approach[20,21]. We use density functional theory within the local density approximation (LDA)[28–30]. Only the valence electrons are treated explicitly, the interaction of the valence electrons with the atomic cores being represented by norm-conserving non-local pseudopotentials[31,32]. The simulations are performed in a periodically repeated cell with the wave functions expanded in plane waves. The basis set includes all plane waves whose kinetic energy is less than a chosen cut-off energy E_{cut}.

An important difference between our calculations and the original Car-Parrinello approach is that instead of treating the electronic degrees of freedom by 'fake dynamics' we relax the electrons to the Born-Oppenheimer surface for every ionic configuration, using conjugate-gradients minimization[33–35]. As in the original scheme, we calculate the forces acting on the ions via the Hellmann-Feynman theorem, and these are then used to integrate the classical equation of motion of the ions. It is computationally more expensive to bring the electrons to the Born-Oppenheimer surface than to do one step in the Car-Parrinello method, but the extra cost is compensated by the fact that we can use a larger molecular dynamics time step. To handle the semi-metallic nature of the system, we use Fermi-surface smearing, with the electronic occupation numbers treated as auxiliary dynamical variables[33,36,37]. A detailed report on how this is done in practice has been presented in our work on ℓ-Ga[38].

Although AIMD has become a standard technique, very few simulations have been reported on systems containing transition or post-transition metals[39,40]. Because of the important role of the d-electrons, it is essential to include them explicitly, and this brings two kinds of problems. Firstly, the number of occupied orbitals is substantially increased. Secondly, the compact nature of the d-orbitals means that a large cutoff E_{cut} is needed, and this implies a large plane-wave basis set. Our AIMD simulations on the Ag-Se system were performed with a version of the CETEP code[41] running on a Cray T3D parallel supercomputer. We note that the version of the code used here reaches the ground state by minimizing with respect to all bands simultaneously, rather than by the band-by-band method of earlier versions. In the liquid simulations, we needed about 12 minimization steps for every ionic configuration to converge the total free energy within 10^{-5} eV/atom.

Technical details of our *ab initio* pseudopotentials are as follows. The Ag pseudopotential has been optimised using the method of Lin *et al.*[42], which is a refinement of the scheme due to Rappe *et al.*[43]. The Se pseudopotential does not require optimisation and the standard Kerker method[44] suffices. For Ag, all states below $4d$, $5s$ and $5p$ are treated as core states. The s and p components of the Ag pseudopotential were generated using the atomic configuration $4d^{10}5s^{0.25}5p^{0.25}$, and the d component using the configuration $4d^{10}5s^{0.5}$. The core radii were 2.0, 2.0 and 2.5 a.u. for the s, p and d components respectively. For Se, we used $4s^2 4p^4$ for the s and p waves and $4s^2 4p^{2.75} 4d^{0.25}$ for the d wave; the core radii were chosen to be 2.0, 2.0, and 2.3 a.u. for the s, p and d components respectively. We work with the pseudopotentials in Kleinman-Bylander separable form[45], with the s-wave treated as local; the non-local parts of the pseudopotentials are treated in real space[46]. We use a plane-wave cut-off of 400 eV. As a preliminary test of our pseudopotentials, we have performed calculations on the low temperature phase α-Ag_2Se, which we present in more detail in the next section. We also tested the pseudopotentials in our work on AgCl[47] and the liquid Ga-Se alloy[26].

III. SOLID Ag_2Se

At atmospheric pressure silver selenide, Ag_2Se, exists in two polymorphic forms. The high temperature form, β-Ag_2Se, is stable above 406 K. The structure is b.c.c. with spacing $a = 4.983$ Å, and the unit cell contains two Ag_2Se units. The Se atoms form a stable b.c.c lattice, while the Ag atoms are statistically distributed among several interstitial sites[48,49]. In this structure, all the Ag atoms are mobile, and in fact α-Ag_2Se is a typical superionic conductor similar to α-AgI and α-Ag_2S[50–52].

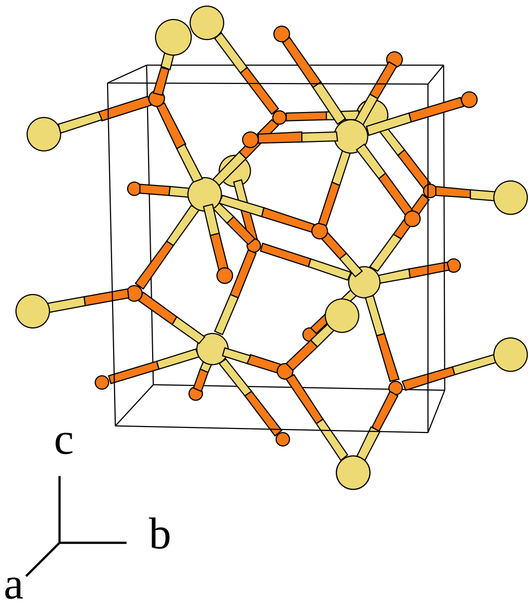

FIG. 1. Arrangement of Ag and Se atoms in solid α-Ag_2Se. Ag and Se atoms are represented by small dark spheres and large light spheres, respectively.

Ag_2Se transforms from the β phase to a low temperature form, α-Ag_2Se, at 406 K. The structure of α-Ag_2Se has been resolved by X-ray powder diffraction as orthorhombic with cell constants $a = 4.333$, $b = 7.062$ and $c = 7.764$ Å. The space group is $P2_12_12_1$ and there are four Ag_2Se units in the unit cell[53]. A three dimensional representation of the structure is shown is in Fig. 1. The four Se atoms are equivalent by symmetry, and they almost lie on two planes perpendicular to the b axis. There are two inequivalent Ag sites. The first type, Ag_{I}, lie just above or below the planes of the chalcogen atoms. These atoms are tetrahedrally coordinated by Se atoms, three in the nearest Se plane and one in the next, at distance 2.62, 2.79, 2.86 and 2.71 Å, respectively. The other silver atoms, Ag_{II}, lie almost halfway between the planes of chalcogen atoms. The arrangement of the Se around the Ag_{II} atoms is almost triangular, at distances 2.72, 2.74 and 2.81 Å, with two second neighbors at 3.28 and 3.50 Å. Each Se atom is surrounded by seven Ag atoms, or nine if the second neighbors are taken into account.

Silver is well known to exist in various solid-state compounds with coordination numbers ranging from 2 up to 8[54]. Examples of coordination 2, 3, and 4 are given by Ag_2O[55], Ag_3AsS_3[56] and AgI[54]. In this respect the binary compounds of silver with the chalcogen elements, Ag_2X (X=O, S, Se and Te), are remarkable since the coordination of silver varies from linear to trigonal bipyramidal when going down the VIa column[53]. With a valence of one for silver these compounds may be regarded as ionic which makes these low coordinations all the more striking, since ionic bonds usually imply higher coordination. The stability of the Ag d^{10} ion in such compounds may be attributed to the mixing of the silver d and s states which occurs when the atom is placed in a low-symmetry environment[57,58].

The electronic properties of α-Ag_2Se are those of a semiconductor with a small energy gap. The exact value of the energy gap, is however controversial, and values ranging from 0.02 to 0.22 eV have been published[6,49].

TABLE I. Comparison of calculated and experimental crystallographic parameters for α-Ag_2Se (experimental values in parentheses). The lattice constants are given in Å . The internal parameters x, y, z are the coordinates of the atoms in units of a, b and c. The three other positions equivalent by symmetry are given by $(\frac{1}{2}+x, \bar{y}, \bar{z})$, $(\bar{x}, \frac{1}{2}-y, \frac{1}{2}+z)$ and $(\frac{1}{2}-x, \frac{1}{2}+y, \frac{1}{2}-z)$.

Lattice constants	a	b	c
	4.218	6.949	7.649
	(4.333)	(7.062)	(7.764)
Internal parameters	x	y	z
Ag_{I}	0.109	0.367	0.455
	(0.107)	(0.366)	(0.456)
Ag_{II}	0.729	0.027	0.362
	(0.728)	(0.029)	(0.361)
Se	0.362	0.245	0.154
	(0.358)	(0.235)	(0.149)

The study of α-Ag_2Se, with three lattice parameters and nine internal parameters to relax, is a stringent test of the quality of our pseudopotentials. All the calculations on α-Ag_2Se were done with a plane-wave cut-off of 400 eV. This cut-off yields well-converged properties of the fully relaxed structure, since increasing E_{cut} to 600 eV changed the forces on the atoms and the stresses on the unit cell only by a negligible amount. The Brillouin zone (BZ) sampling was performed using a Monkhorst-Pack special k-points mesh[59]. We also had to introduce a Gaussian smearing of the Fermi surface[33] due to the absence of a real gap in the system. We had to use a (4×4×4) grid (equivalent to 8 k-points in the irreducible part of the BZ) for the energy per atom to be converged within a few meV. The energy broadening we used was 0.2 eV.

We performed a full structural relaxation of the crystal structure by varying the three lattice parameters and the nine independent internal parameters. In Tab. I, the calculated lattice constants and internal parameters are compared with experiment. The lattice parameters are in satisfactory agreement with experiment, being too low by ∼2%, which is typical of LDA calculations. The experimental internal parameters for the Ag atoms are very well reproduced. For the Se atoms however, the relaxations were larger, and this leads to larger discrepancies with experiment. The resulting Ag-Se distances compared with experimental values are (Å units): 2.68 (2.62), 2.72 (2.78), 2.89 (2.86), 2.80 (2.71) for Ag_{I} and 2.67 (2.74), 2.74 (2.72) and 2.80 (2.81) for Ag_{II}.

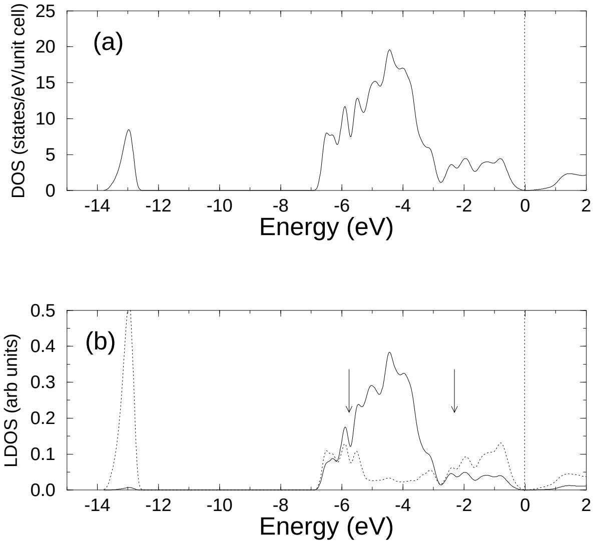

FIG. 2. (a) Electronic density of states of solid α-Ag_2Se and (b) local density of states on the Ag (full line) and Se (dotted line) sites. The arrows indicate the energies of the states analysed in Fig. 3.

In Fig. 2a, we show the electronic density of states (DOS) of α-Ag_2Se. The local densities of states (LDOS) shown in Fig. 2b allow us to identify the main features of the DOS. The Se(4s) states give rise to the lowest peak at –12.5 eV, while the large peak below –4 eV originates from the Ag(4d) states. This prominent peak is superimposed on a broader feature extending from –6.5 eV up to the Fermi level, which arises from the Se(4p) states. Even though the DOS is very small at the Fermi level, there is no real gap in the system. This is not surprising in view of the very small value of the experimental gap (less than 0.25 eV) and the well known tendency of DFT to give energy gaps that are too small. An examination of the band structure reveals that the states at the Fermi level are situated around the Γ point in the BZ.

The LDOS reveals that the Se(4p) band is composed of two peaks situated at –5.5 eV and –1.5 eV. These peaks coincide with features in the LDOS on the silver atoms, which exhibits an asymmetric shoulder below its main peak and has a tail that extends from –3 eV up to the Fermi level. We believe this to be a signature of hybridization between the Ag(4d) and the Se(4p) states. This hypothesis is clearly supported by examining density plots arising from single bands.

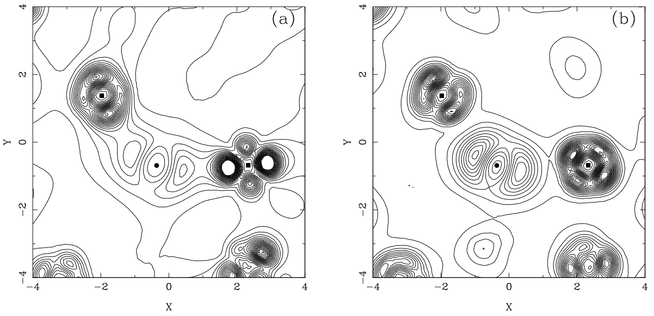

FIG. 3. Square of Kohn-Sham orbital from two bands with energies of –5.76 and –2.30 eV respectively. The orbitals are plotted on a plane passing through a Se (circle) and two neighboring Ag (square).

In Fig. 3 we show the densities of two states, in a plane passing through a Se atom and two neighboring Ag atoms. The energies of the two states are indicated by arrows in Fig. 2. For both energies, the density is distributed over both the Se and the Ag atoms. The wavefunction clearly has a p character on the Se, whereas on the Ag sites the four visible lobes indicate a pronounced d-like character.

An alternative way of looking at the bonding in a solid is to examine how the charge is redistributed with respect to neutral atoms. A careful analysis of this charge redistribution in α-Ag$_2$Se shows that the region where the electron density has been enhanced is centered on the Se atoms and is broadly – almost spherically – spread between the Se and its nearest Ag atoms. This nondirectional character of the bonds together with the high coordination of Se are compatible with ionic bonding.

The picture that emerges is thus a valence band consisting of Se(4s), Se(4p) and Ag (4d) states with strong hybridization between the latter two. The empty states above the Fermi level can be seen as Ag(5s/p) states, presumably hybridized quite strongly with Se(4p). With the Se(4p) band filled and the Ag(5s/p) states empty we thus arrive at a (partially) ionic model for the stoichiometric solid.

IV. LIQUID ALLOYS

A. Details of the simulations

Our simulations of the Ag-Se liquid alloys have been performed on a system of 69 atoms in a cubic box with periodic boundary conditions. The wave-functions are expanded in plane waves with the same cutoff of 400 eV as before; this implies a basis set of $\sim$ 28,000 plane waves for the whole system. We included only the Γ-point to sample the Brillouin zone, and we used a Fermi-smearing energy width of 0.2 eV, as for the solid. The Verlet algorithm was used to integrate the ionic equation of motion, with a time step of 3 fs. We have performed simulations at the temperature $T \simeq 1350$ K for three concentrations of Ag$_{1-x}$Se$_x$, namely: $x = 0.33$ (46 Ag atoms and 23 Se atoms), $x = 0.42$ (40 Ag atoms and 29 Se atoms) and $x = 0.65$ (24 Ag atoms and 45 Se atoms). The simulations were performed at a density which is linearly interpolated between experimental values for ℓ-Ag$_2$Se[60] and ℓ-Se[12].

To initiate the simulations, we exploited the fact that an empirical pair-potential model[22] has been developed for the stoichiometric Ag$_2$Se system. This is a partially ionic model which reproduces the structure of the liquid reasonably when used in classical molecular dynamics – a direct comparison of the model with our AIMD simulations will be presented later. We began by making simulations with this empirical model, and we then switched over to AIMD and let the system equilibrate for a further 1 ps before collecting data over the next 2 ps. We reached the other Ag$_{1-x}$Se$_x$ compositions by replacing some of the Ag atoms by Se atoms and then equilibrating for 1 ps at the new composition; production runs of 1-2 ps were again performed in each case.

B. Structural properties

1. Structure factors

The most direct and detailed way to compare our simulations with experiment is through the static structure factors, which have been measured for the stoichiometric composition Ag$_2$Se. The neutron-weighted structure factor $S_n(k)$ was measured some years ago[13], and very recently the partial structure factors $S_{\alpha\beta}(k)$ have also been measured, using the technique of isotope substitution[14].

The definition of $S_{\alpha\beta}(k)$ used here to compare with experiment is that due to Faber and Ziman[61], according to which:

$$S_{\alpha\beta}(k) = (\langle \rho_\alpha^*(\boldsymbol{k}) \rho_\beta(\boldsymbol{k}) \rangle - \delta_{\alpha\beta}) / \sqrt{c_\alpha c_\beta}, \qquad (1)$$

where c_α is the concentration of species α, $\rho_\alpha(\boldsymbol{k})$ represents the Fourier transform of the number density of species α, and the angular brackets indicate the thermal average. With this definition, the neutron-weighted structure factor is given by:

$$S_n(k) = \frac{\sum_{\alpha\beta} c_\alpha c_\beta b_\alpha b_\beta S_{\alpha\beta}(k)}{\sum_\alpha c_\alpha b_\alpha^2} + 1, \qquad (2)$$

where b_α is the coherent scattering length of species α. We use the scattering lengths $b_{\mathrm{Ag}} = 5.98$ fm and $b_{\mathrm{Se}} = 7.97$ fm[1,13].

Comparisons of the structure factors given by simulation and experiment are shown in Fig. 4. Agreement between the two for $S_n(k)$ is very good, with all the main peaks having the correct position and height. The excellent agreement of the period, amplitude and phase of the oscillations at larger wavevectors is particularly gratifying. Our results also reproduce the small pre-peak at $k \simeq 1.7$ Å^{-1}, though its magnitude is somewhat lower than the experimental value.

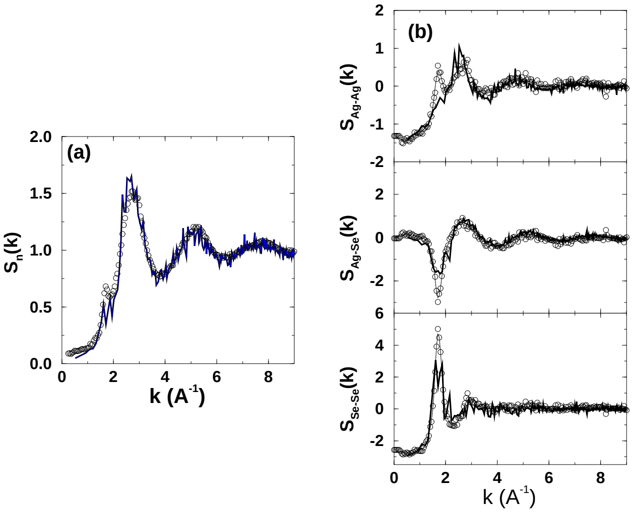

FIG. 4. (a) Comparison of the calculated total neutron weighted structure factor $S_n(k)$ of $\mathrm{Ag_2Se}$ with the experimental results[1]. (b) The measured partial structure factors $\mathrm{S}_{\alpha\beta}(k)$ of $\mathrm{Ag_2Se}$[14] compared with those extracted from our simulation. The theoretical curves are shown in thick lines, those from experiment with circles (the thin line is a smoothed version of the experimental curve).

However, the more detailed comparisons allowed by the $S_{\alpha\beta}(k)$ structure factors reveal some discrepancies. The most noticeable is the absence of the pre-peak at $k \simeq 1.7$ Å^{-1} in our $S_{\mathrm{Ag-Ag}}(k)$. There are also substantial differences in the magnitudes of the peaks in $S_{\mathrm{Ag-Se}}(k)$ and $S_{\mathrm{Se-Se}}(k)$ at this wavevector. Since we found a discrepancy in $S_n(k)$ at the same wavevector, the problem is unlikely to be due to the experimental analysis of the structure factor into partials. Our initial suspicion was that the small size of our system might be responsible for the discrepancy. However, we have tested this idea by doing simulations with the empirical model for different sizes of system, and these tests give no indication of significant differences between the 69-ion system and much larger systems. It is possible that fluctuations at the wavevector in question are very slow and that our simulations are not long enough to achieve adequate statistics for such long wavelengths.

2. *Pair correlation functions*

Our calculated partial radial distribution functions (RDF) $g_{\mathrm{Ag-Ag}}(r)$, $g_{\mathrm{Ag-Se}}(r)$ and $g_{\mathrm{Se-Se}}(r)$ for the stoichiometric composition are reported in Fig. 5, where we compare with the neutron diffraction results of Lague *et al.* [14], and with the predictions of the empirical interaction model[22] mentioned earlier.

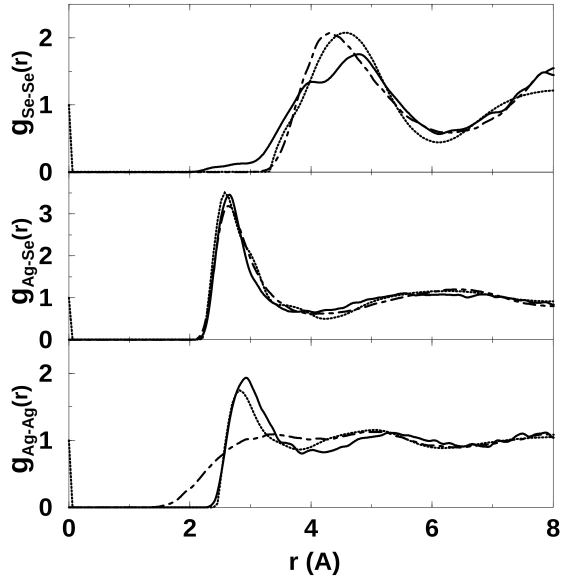

FIG. 5. Calculated partial radial distribution functions $g_{\alpha\beta}(r)$ of $\mathrm{Ag_2Se}$ (full lines) compared with the results of experiment[14] (dotted lines) and the predictions of an empirical ionic model[22] (dash-dotted lines).

The agreement of our simulated RDFs with experiment in the region of the first peak is excellent for Ag-Se and reasonably good for Ag-Ag, but in both cases there are quite noticeable differences at larger distances, as would be expected from the discrepancies of the corresponding $S_{\alpha\beta}(k)$ at $k \simeq 1.7$ Å^{-1}. The agreement with experiment is somewhat less good for $g_{\mathrm{Se-Se}}(r)$, and there is no sign in the experimental results of the doubling of the first peak observed in our simulations, or of the weak distribution we find for $r < 3$ Å. We return below to the meaning of the latter. If we are correct in attributing discrepancies in the structure factors at low k to inadequate sampling, then discrepancies in the RDFs at large r are presumably due to the same effect. However, the differences of simulated and experimental $g_{\mathrm{Se-Se}}(r)$ around the first peak must have a different explanation, and we do not at present know what this is.

Our comparisons show that the empirical interaction model performs extremely well for $g_{\mathrm{Ag-Se}}(r)$, but differs greatly from both the experimental and AIMD results for $g_{\mathrm{Ag-Ag}}(r)$. It seems certain that the model is seriously mis-representing the Ag-Ag interaction at short distances. Interestingly, for $g_{\mathrm{Se-Se}}(r)$, the model agrees somewhat better with experiment than our AIMD results around the first peak.

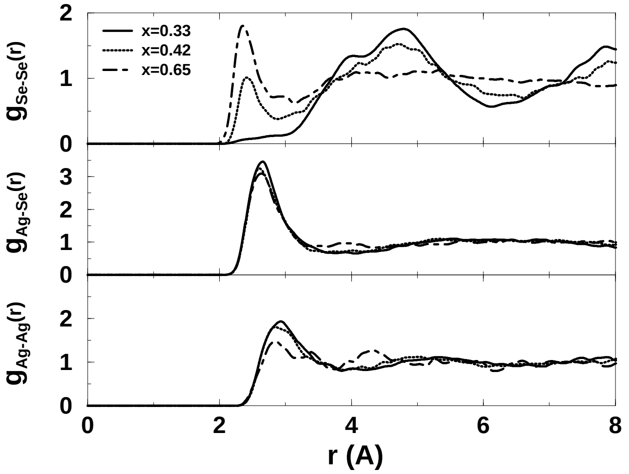

FIG. 6. Partial radial distribution functions $g_{\alpha\beta}(r)$ from simulated ℓ-$\mathrm{Ag}_{1-x}\mathrm{Se}_x$ at concentrations x=0.33 (full line), x=0.42 (dotted line) and x=0.65 (dot-dashed line).

We show in Fig. 6 how the partial RDFs change with composition according to the AIMD simulations. The results show that increase of Se content causes dramatic changes in $g_{\text{Se-Se}}(r)$. At stoichiometry, $g_{\text{Se-Se}}(r)$ exhibits broad peaks at 3.99 and 4.83 Å, and only a very weak tail below 3.0 Å. For $x = 0.42$, instead of a tail, there is a short-distance peak at 2.35 Å. The position of the main peak has shifted to 4.72 Å and has decreased in magnitude. The peak around 4.0 Å seen at stoichiometry has merged with the main peak to give rise to a shoulder. At the last concentration, the short-distance peak is dominant and $g_{\text{Se-Se}}(r)$ shows little structure beyond 4.0 Å, with a low and broad second peak.

The mechanism behind the changes observed in $g_{\text{Se-Se}}(r)$ is the tendency of Se to bond to itself as x exceeds 0.33, and it is no coincidence that the position of the short-distance peak is almost the same as the Se-Se covalent bond lengths in crystalline and liquid Se, which are equal to 2.37 Å[62] and 2.34 Å[16] respectively. The nature of this peak can be probed by analysing the coordination of the selenium atoms. In general, we define the α-β coordination as the average number of neighbouring β atoms within a sphere of radius r_c around an α atom. The growth of the short-distance peak can be characterized by the Se-Se coordination, which, for $r_c = 2.9$ Å, we calculate to be 0.1, 0.6 and 1.5 for $x = 0.33$, 0.42 and 0.65 respectively. Thus the coordination grows as x increases, reflecting the tendency of Se atoms to form bonds. This will become even clearer when we examine the electronic structure of the liquid below. In comparison to the modifications observed in $g_{\text{Se-Se}}(r)$, $g_{\text{Ag-Se}}(r)$ is hardly affected by the change of composition. The magnitude of the main peak decreases slightly with increasing x and its position varies only a little: 2.65, 2.60 and 2.64 Å for $x = 0.33$, 0.42 and 0.65 respectively. At stoichiometry, a very broad second peak may be distinguished around ~ 6 Å, but it progressively disappears with increasing x, and at $x = 0.65$ $g_{\text{Ag-Se}}(r)$ is nearly constant for $r > 4.0$ Å. A similar gradual loss of structure is observed for the Ag-Ag pair correlation function as the height of the first peak decreases with increasing Se concentration. This is accompanied by a slight shift of the first peak of $g_{\text{Ag-Ag}}(r)$ to smaller r. For $x = 0.65$ we note the presence of many oscillations in $g_{\text{Ag-Ag}}(r)$. These may partly be due to the small number of silver atoms at this concentration and the resulting poorer statistics for the Ag-Ag pair correlation function. However, the absence of structure in $g_{\text{Ag-Ag}}(r)$ at this concentration clearly indicates that the arrangement of the Ag atoms is very disordered. Furthermore, the low magnitude of the first peak suggests that the Ag atoms are in fast exchange with their first coordination shell, and that the Ag atoms are likely to be very mobile. The characteristic interatomic distances and coordination numbers deduced from the partial RDFs are summarized in Table II, together with those found in both the low temperature (α-$\mathrm{Ag_2Se}$) and the superionic (β-$\mathrm{Ag_2Se}$) phases of $\mathrm{Ag_2Se}$.

TABLE II. Inter-atomic distances and coordination numbers in simulated ℓ-$\mathrm{Ag}_{1-x}\mathrm{Se}_x$ and in the crystalline phases α-$\mathrm{Ag_2Se}$ and β-$\mathrm{Ag_2Se}$. $r_{\alpha\beta}$ is the first neighbor distance between species α and β. $r^c_{\alpha\beta}$ is the cut-off radius used for calculating the coordination number $n_{\alpha\beta}$. All distances are given in Å.

Phase	$x = 0.33$	$x = 0.42$	$x = 0.65$	α-$\mathrm{Ag_2Se}$	β-$\mathrm{Ag_2Se}$
$r_{\mathrm{Ag-Ag}}$	2.93	2.84	2.85	2.93	3.15
$r_{\mathrm{Ag-Se}}$	2.65	2.60	2.64	2.62	2.70
$r_{\mathrm{Se-Se}}$	3.99,4.83	2.41,4.72	2.35	3.98,4.59	4.30
$r^c_{\mathrm{Ag-Ag}}$	3.90	3.93	3.76	3.68	4.35
$r^c_{\mathrm{Ag-Se}}$	3.77	3.65	3.62	2.90	3.45
$r^c_{\mathrm{Se-Se}}$	2.9,6.12	2.90	2.90	5.14	6.00
$n_{\mathrm{Ag-Ag}}$	6.6	3.4	2.0	6	10
$n_{\mathrm{Ag-Se}}$	3.8	4.0	5.1	3.5	4
$n_{\mathrm{Se-Se}}$	0.1,13.6	0.6	1.5	14	14

It is interesting to notice that the distances and coordination found for $x = 0.33$ are very close to those found in the low temperature phase. In particular, the positions of the two superimposed peaks in $g_{\text{Se-Se}}(r)$ are similar to the two nearest Se-Se distances found in the solid. This is surprising, since one would rather expect the melt to resemble the disordered superionic phase, in which the Ag ions diffuse through a b.c.c. Se lattice.

3. Analysis of the Se structure

The growth of the short-distance peak in $g_{\mathrm{Se-Se}}(r)$ with increasing Se content is due to the formation of Se clusters for $x > 0.33$. The simplest way to see this is by studying 'ball-and-stick' pictures for typical configurations. Fig. 7 displays examples of such pictures for the three compositions. In constructing these pictures, pairs of Se atoms are joined by sticks if their separation is less than 2.9 Å, this distance being chosen because it is close to the first minimum of $g_{\mathrm{Se-Se}}(r)$ for $x =$ 0.42 and 0.65. At stoichiometry, very few Se clusters are present, with only the occasional dimer (Fig. 7a), and the even more occasional trimer. It is the presence of these small clusters that gives rise to the weak tail in $g_{\mathrm{Se-Se}}(r)$ at low r. For $x = 0.42$, the Se atoms bond not only into dimers and trimers but also into larger Se$_n$ clusters (see Fig. 7b). At this composition, some $\sim$ 48 % of the Se atoms are bonded, with 76 % of these one-fold and 22 % two-fold coordinated, with the remaining 2 % having higher coordination.

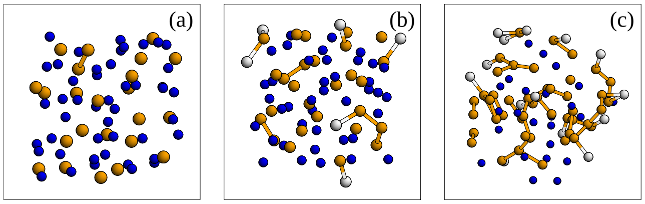

FIG. 7. Snapshots of typical configurations of ℓ-Ag$_{1-x}$Se$_x$ at concentrations (a) x=0.33, (b) x=0.42 and (c) x=0.65. Silver atoms are shown as black spheres, selenium atoms as gray spheres. Bonds are drawn between Se atoms with separation < 2.9 Å. Bonds to atoms in neighboring cells are represented with two-colored sticks.

TABLE III. Distribution of coordination numbers $n_{\mathrm{Se-Se}}$ at x=0.33, 0.42 and 0.65. We show the average percentage of atoms with coordination N_c.

N_c	$x = 0.33$	$x = 0.42$	$x = 0.65$
0	93	52	9
1	6	36	46
2	<1	10	38
3	-	<2	6
≥4	-	-	<1

The dominance of one-fold and two-fold coordination means that most of the clusters are either dimers or Se$_n$ *chains*. At the composition $x = 0.65$, most of the Se atoms are in clusters, with an average of 7 % being isolated (see Fig. 7c). The proportions of bonded Se with one-fold and two-fold coordination are now 35 % and 40 %, with a rather significant percentage (15 %) of three-fold coordinated atoms. In Table III, we summarize the distribution of first-neighbor Se-Se coordination numbers, for all three concentrations.

To understand the structure of the Se clusters in more detail, we have studied their size distribution. In Fig. 8, we display the average numbers of clusters present in our sample *versus* the number of Se atoms n in the cluster. For all three concentrations, dimers are the most common clusters. The number of clusters drops rapidly with increasing n. For $x = 0.42$, the prevalent clusters contain up to 5 atoms. Only a very small number of clusters with $n > 5$ was found, the largest being $n = 9$. When the Se content increases to $x = 0.65$, the cluster-size distribution broadens substantially. The largest cluster present in our sample was $n = 28$, but all clusters with $n < 10$ are very frequent.

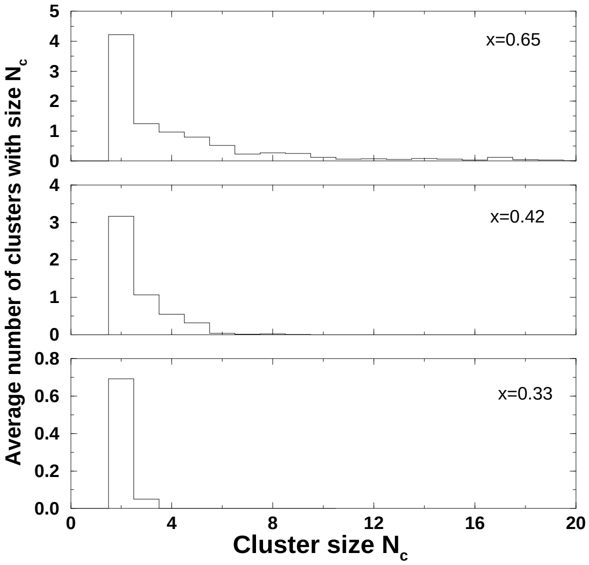

FIG. 8. Average number of Se clusters of size n in ℓ-Ag$_{1-x}$Se$_x$ at concentrations x=0.33, 0.42 and 0.65 (full line).

An analysis of the structure of the clusters reveals that there is a simple relationship between the number of bonds within a cluster N_b and the number of atoms composing that cluster n. We found that for over 95 % of the clusters we have $N_b = n - 1$, at all three concentrations. The significance of this is that the relation $N_b = n - 1$ indicates a tree-like topology without closed loops. Almost all the exceptions to this are clusters with $N_b = n$, which indicates the existence of a single closed loop. We note that, for large clusters, loops defined in this way may occur simply as an artifact of the periodic boundary conditions. In any case, the conclusion is clear: loops are rare.

C. Dynamical properties

We have studied the diffusion of atoms in the liquid by calculating the time-dependent mean square displacement (MSD), defined in the usual way for species α as:

$$\langle \Delta r_\alpha(t)^2 \rangle = \frac{1}{N_\alpha} \left\langle \sum_{i=1}^{N_\alpha} |\mathbf{r}_{\alpha i}(t+t_0) - \mathbf{r}_{\alpha i}(t_0)|^2 \right\rangle \ , \qquad (3)$$

where the sum goes over all N_α atoms of species α, t_0 is an arbitrary time origin, and the angular brackets denote a thermal average, or equivalently an average over time origins. For diffusing systems, the MSD is linear in t for large $|t|$, and the slope is proportional to the self-diffusion coefficient D_α of species α:

$$\langle \Delta r_\alpha(t)^2 \rangle \to 6 D_\alpha |t| + B_\alpha \ , \qquad (4)$$

where B_α is a constant.

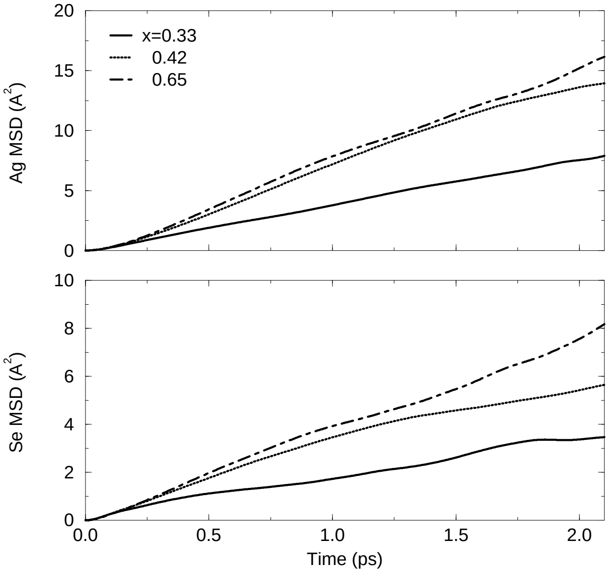

FIG. 9. Mean square displacement $\langle \Delta r_\alpha(t)^2 \rangle$ of Ag (top panel) and Se (lower panel) in ℓ-Ag$_{1-x}$Se$_x$ for x=0.33 (full lines), 0.42 (dotted lines) and 0.65 (dash-dotted lines).

We have calculated the MSD for Ag and Se for the three compositions, by averaging over the atoms of each species and over time origins. Our calculated MSDs are graphed in Fig. 9, and the estimated diffusion coefficients are reported in Table IV. In all normal liquids, the asymptotic linear behavior of $\langle \Delta r_\alpha(t)^2 \rangle$ is attained after only a few tenths of a ps, and this is the behavior we find. The lack of straightness of the curves at long times is simply an effect of statistical averaging (the ideal asymptotic form shown in Eqn. (4) assumes perfect averaging over a simulation of infinite duration). The slopes used to obtain the values of D_α were estimated by a least-square fitting of a line to the data.

Our results show three things: the diffusion coefficients are similar to those of other normal liquids, being in the range 10^{-5} – 10^{-4} cm^{2}s^{-1}; Ag diffuses faster than Se; and the diffusion of both species increases with Se content. Unfortunately, there appear to be no experimental data for the diffusion coefficients. However, D_{Ag} has been measured in the superionic phase of the β-Ag$_2$Se crystal[63,64]. This is relevant, because it is commonly found that the diffusion coefficients of the mobile species in superionic conductors change only a little on melting. The measured value of D_{Ag} in superionic β-Ag$_2$Se at the melting point is 6×10^{-5} cm^{2}s^{-1}[63], which is rather close to our calculated value of 6.4×10^{-5} cm^{2}s^{-1} for the stoichiometric liquid. It is also relevant to note that the empirical interaction model[22] reproduces the experimental values of D_{Ag} in β-Ag$_2$Se quite well. This model predicts the values $D_{\text{Ag}} = 10.6 \times 10^{-5}$ cm^{2}s^{-1} and $D_{\text{Se}} = 3.4 \times 10^{-5}$cm^{2}s^{-1} for ℓ-Ag$_2$Se at $\sim$ 1380 K[22,65], which are quite close to our AIMD values. However, we believe that too much weight should not be put on this comparison, because of the rather poor results for $g_{\text{Ag}-\text{Ag}}(r)$ given by the empirical model.

Even though experimental values for the D_α are not available, there have been measurements of the ionic conductivity σ_i, i.e. the electrical conductivity measured under conditions such that the flow of electrons is blocked. A rough check against our calculated D_α can be made using the approximate Nernst-Einstein relation:

$$\sigma_i = (k_B T)^{-1} \sum_\alpha \bar{\rho}_\alpha (z_\alpha e)^2 D_\alpha \ , \qquad (5)$$

where $\bar{\rho}_\alpha$ is the bulk number density of species α and z_α is its ionic charge. This relation is based on the assumption that ions diffuse independently of one another. The check can only be rough since it is not clear exactly what values should be assumed for z_α. However, if we assume full ionicity ($z_{\text{Ag}} = +1$, $z_{\text{Se}} = -2$), then our calculated values of D_α for the stoichiometric composition lead to a predicted σ_i of 4.9 Ω^{-1}cm^{-1}, which is rather close to the measured value of 5.2 Ω^{-1}cm^{-1}[5,63,64].

TABLE IV. Self-diffusion coefficients D_α of Ag and Se in ℓ-Ag$_{1-x}$Se$_x$ for x=0.33, 0.42 and 0.65 in units of 10^{-5} cm^{2}s^{-1}.

x	0.33	0.42	0.65
D_{Ag}	6.4	11.2	13.1
D_{Se}	2.7	4.2	6.3

Our finding that D_{Ag} and D_{Se} increase with Se content is surprising at first sight, since we have seen that Se forms large clusters when $x > 0.3$. As noted in the Introduction, the chain-like nature of pure ℓ-Se is also well established. It would be expected that the formation of covalently bonded clusters would make it more difficult for Se atoms to diffuse, and that the chain-like network would also hinder the diffusion of Ag. However, this depends very much on the stability of the chains, in other words on the lifetime of the covalent bonds.

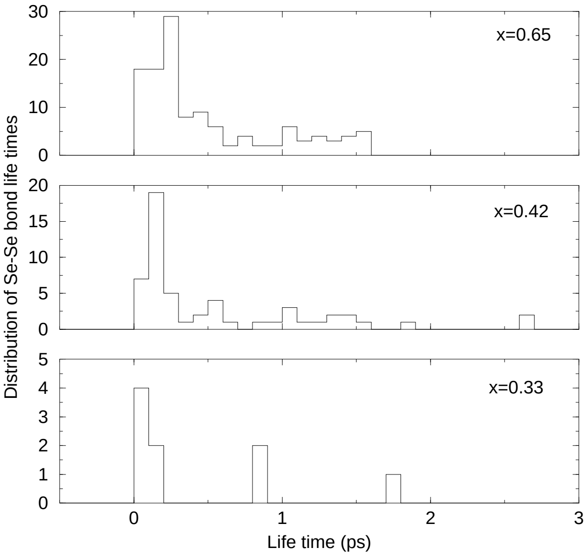

FIG. 10. Distribution of Se-Se bond lifetimes in ℓ-$\mathrm{Ag}_{1-x}\mathrm{Se}_x$ for x=0.33, 0.42 and 0.65.

In order to pursue this question further, we have analyzed our simulations to estimate the Se-Se bond lifetime. To define the lifetime of a bond between two atoms, we regard the bond as being made when the distance between the atoms becomes less than a creation distance r_1; it is broken when the distance becomes greater than a somewhat larger cut-off r_2. We decided to adopt this definition involving two cutoff radii because there are large fluctuations in the distance between bonded atoms, and we do not wish to count a bond as broken simply because the distance momentarily exceeds the creation distance r_1. In fact, our conclusions would not be significantly affected if we put $r_1 = r_2$. The distribution of bond lifetimes obtained for $r_1 = 2.9$ Å and $r_2 = 3.2$ Å is shown for all three compositions in Fig. 10. The distributions are very broad, with lifetimes ranging from less than 0.1 ps up to 2.6 ps. For the majority of bonds, the lifetime is less than 1.0 ps. For $x = 0.42$ and 0.65, the average lifetimes are 0.52 and 0.50 ps respectively. (The number of Se-Se bonds in the stoichiometric case was too small to give a statistically meaningful lifetime.) These rather short bond lifetimes make it less surprising that the diffusion coefficients increase with increasing Se content.

D. Electronic properties and bonding

In this section we will examine how the structural changes are linked to the electronic properties of the liquid alloy. The calculated electronic DOS for the three compositions are shown in Fig. 11a. The states can be classified as: Se($4s$) states around −12 eV, Ag($4d$) states at −4 eV and Se($4p$) states in the region above −7 eV. The identification of these features is made straightforward by the examination of the LDOS on the Ag and Se atoms, which are displayed in Fig. 11b.

The DOS and LDOS for ℓ-$\mathrm{Ag}_2\mathrm{Se}$ are very similar to those found for α-$\mathrm{Ag}_2\mathrm{Se}$ (see Sec. III). In particular, the hybridization of Se($4p$) states with Ag($4d$) states is also found in the liquid, as is clear from the asymmetry of the Ag($4d$) band and the dumbbell-shaped Se($4p$) band. We note however an increase in the DOS in the region of the Fermi energy on going from solid to liquid.

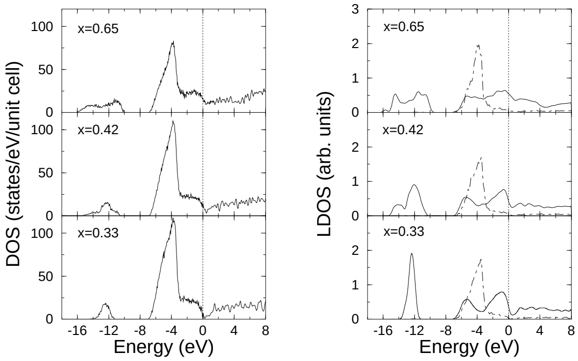

FIG. 11. Density of states (left panel) and local densities of states (right panel) for Ag (chain curve) and Se (dotted curve) from simulations of $\mathrm{Ag}_{1-x}\mathrm{Se}_x$ at $x = 0.33$, 0.42 and 0.65. For clarity, the scale used for the Se LDOS is four times that used for the Ag LDOS. The vertical dotted line marks the Fermi energy.

Even though the DOS for the three concentrations are quite similar, we observe significant modifications as the Se concentration is changed. First, the height of the sharp Ag($4d$) peak decreases with respect to the higher peak of the Se($4p$) band which remains the same. Second, the Se($4s$) band which is narrow and has a single peak at stoichiometry becomes substantially broader and splits into two peaks as x is increased. Finally, the DOS at the Fermi level (E_{F}) increases with x and the pseudogap present at x=0.33 becomes shallower.

The LDOS reveal the nature of these changes. We see that the shape of the Ag LDOS is essentially identical for all three concentrations. In particular, the asymmetry of the main peak is present for all x, which means that the Ag($4d$)-Se($4p$) hybridization is unaffected by changes in the concentration. The rigidity of the Ag LDOS thus implies that the modifications in the DOS are mainly due to the changes in the LDOS of Se. There are indeed large changes in the Se LDOS as x changes from 0.33 to

0.65: the two peaks of the p band are smeared out and a third peak appears above the Fermi level. The first and third peaks are situated symmetrically about the middle peak and are approximately of the same magnitude. The structure of the Se LDOS at $x = 0.42$ may simply be described as intermediate between these two cases, as can be seen from the Se($4s$) states. For all three concentrations, we see that the states at E_{F} arise from the Se($4p$) band. Thus the increase of the DOS at the Fermi level is clearly due to the broadening of the second Se($4p$) peak, and to the presence of the third peak which both effectively reduce the depth of the pseudo-gap.

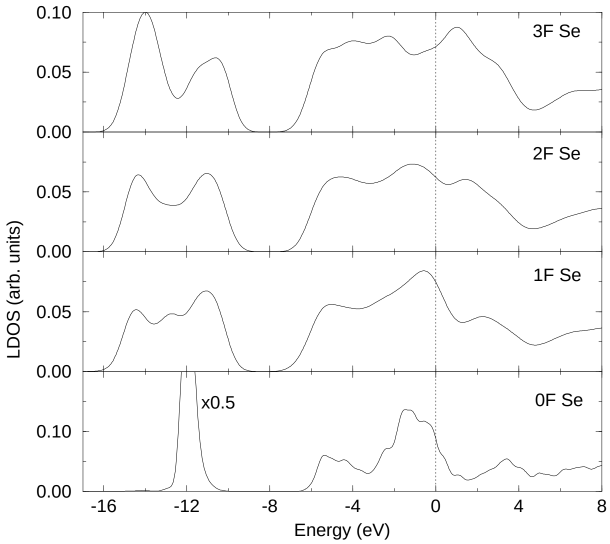

FIG. 12. Decomposition of the Se LDOS into contributions from isolated (0F), one-fold (1F), two-fold (2F) and three-fold (3F) coordinated Se atoms.

All these changes are closely related to the modifications of the structure. Our interpretation of the changes is as follows. The presence of a pseudo-gap and the low value of the Se LDOS above the Fermi level at the stoichiometric composition suggest that all the Se($4p$) states are filled, so that there are 6 p-electrons per Se atom. This corresponds to an ionic model in which it is energetically favorable for the Ag($5s$) electrons to transfer to empty Se($4p$) states, since the atomic Ag($5s$) state is higher in energy than the Se($4p$) states. This corresponds to a charge transfer from the Ag to the Se ions, thus leading to Ag^{+} ions and Se^{2-} ions. This naturally leads one to interpret the states above E_{F} as being Ag($5s$-p) states, so that the picture here is essentially the same as for the solid, where we have already seen that an ionic model is appropriate. As x increases beyond 0.33, the number of occupied $4p$ states per Se atom falls below 3 due to the creation of Se-Se bonds. The formation of these bonds is clearly illustrated by the appearance of the third peak above the Fermi level, which corresponds to the anti-bonding states, the first and second peak corresponding to bonding and lone-pair states, respectively. The anti-bonding states are hybridized with Ag($5s$-p) states, and only become clearly visible at $x = 0.65$. The formation of Se-Se bonds is also reflected by the splitting of the Se($4s$) which arises from the formation of bonding and anti-bonding Se($4s$) combinations in the clusters.

To show more clearly the effect of the formation of Se-Se bonds on the Se LDOS, we have decomposed this LDOS for $x = 0.65$ into contributions from isolated, one-fold, two-fold and three-fold coordinated Se atoms, as shown in Fig. 12 (we denote these different coordinations as 0F, 1F, 2F and 3F). We note the strong resemblance of the LDOS for the isolated atoms with the Se LDOS for the stoichiometric composition, with the Fermi close to minimum of the LDOS. For 2F atoms, the Se($4s$) band has split symmetrically into bonding and anti-bonding states, while the Se($4p$) now consists of three peaks, which we have identified above as bonding, non-bonding (lone pair) and anti-bonding. The Fermi energy in this case falls roughly between non-bonding and anti-bonding states, as we would expect in a chain-like structure[66]. The LDOS for 1F atoms is intermediate between the 0F and 2F forms; the Se($4p$) bonding and anti-bonding peaks are weaker than for the 2F atoms, since only one bond is involved. Note that if E_{F} fell exactly at the top of the non-bonding peak the number of electrons in the occupied Se($4p$) states would give the 0F, 1F and 2F atoms charges of –2, –1 and 0 respectively.

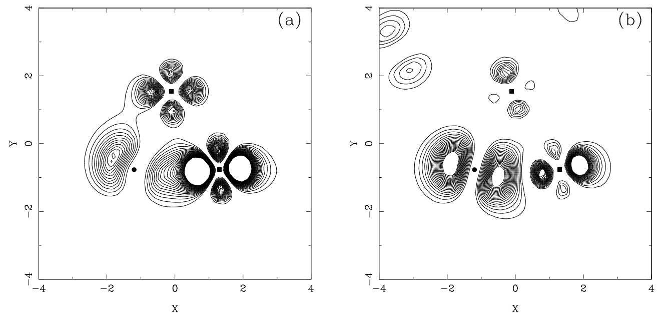

FIG. 13. Square of Kohn-Sham orbital from two individual bands with energies of –5.3 (a) and –1.0 eV (b) respectively. The orbitals are plotted on a plane passing through a Se (circle) and two neighboring Ag (square). The hybridized nature of the states is clearly visible, with a p and d character of the wave functions on the Se and Ag atoms respectively. The hybridization has a bonding character for the lowest states and is anti-bonding for the highest states.

Several features of the DOS and LDOS can be confirmed by a study of the electron density. A useful way to do this in the liquid is to examine the density in a plane passing through three neighbouring atoms. The presence of hybridization of the Se($4p$) states with Ag($4d$) states is illustrated in Fig. 13 which shows the density of one state from the bottom and another from the top of the Se($4p$)/Ag($4d$) band at –5.3 eV and –1.0 eV, respectively.

The very close resemblance of these density distributions to those found in the crystal (see Fig. 3) shows that this aspect of the electronic structure persists essentially unchanged in the liquid state. In the ionic model we propose the states in the Ag LDOS above the the Fermi level arise from the empty silver *s* states. This is confirmed by the charge density of a state at 2 eV above the Fermi level shown in Fig. 14. The wave function has a clear *s* character on the Ag atom and is slightly hybridized with Se(4*p*) states.

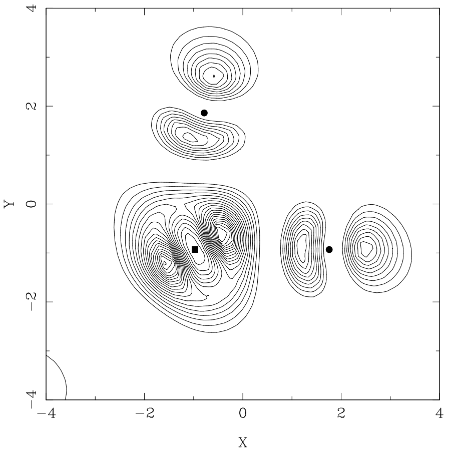

FIG. 14. Square of Kohn-Sham orbital of a state from the conduction band with an energy of 3.5 eV. The orbitals is plotted on a plane passing through a Ag (square) and two neighboring Se (circle). This state is mainly localised on the Ag atoms and has a clear *s* character. This supports the ionic model in which the silver atoms have lost their *s* electrons to become Ag^+ ions.

We have calculated the electronic conductivity σ in our simulations by the Kubo-Greenwood formula[67] as has been done in several previous *ab initio* calculations[23,26,68,69]. Our results are shown in Table V where they are compared with recent experimental measurements made over the whole composition range[7,8]. We have included in the table a calculated result for the conductivity of ℓ-Se taken from our own unpublished AIMD simulation performed at 1370 K[70], since this will be relevant to the discussion.

TABLE V. Calculated conductivity (units of $\Omega^{-1}\mathrm{cm}^{-1}$) using the Kubo-Greenwood formula compared with experimental data[8] at different compositions x.

x	Theory	Expt.
0.33	480	410
0.42	1500	300
0.65	1250	490
1.00	400[a]	∼1[b]

[a] Ref.[70]

[b] Ref.[10]

The conductivity $\sigma = 480\Omega^{-1}\mathrm{cm}^{-1}$ found at stoichiometry is in satisfactory agreement with the experimental data. However, as x increases, the calculated σ first increases dramatically to $\sim$1500 $\Omega^{-1}\mathrm{cm}^{-1}$ at $x = 0.42$ and then decreases slightly to $\sim$ 1250 $\Omega^{-1}\mathrm{cm}^{-1}$ at $x = 0.65$. These values are 3-4 times higher than the experimental values. For pure ℓ-Se the calculated σ is too large by at least two orders of magnitude. We believe that these large discrepancies with experiment arise from the approximations implicit in the Kubo-Greenwood approach. There are two major deficiencies in the Kubo-Greenwood formula as applied here. First, it completely ignores electron-electron collisions, and includes only the effect of scattering of the electrons by the ions. Second, and much more serious, it works with the Kohn-Sham energies, rather than with quasi-particle energies. For metallic systems having free-electron-like DOS, the errors are probably small, and in cases like ℓ-Si[68] and ℓ-Ga[38] the method has been shown to work well. But in systems having a pseudogap, like the liquid alloys considered here, the use of the (artificial) Kohn-Sham energies is very likely to cause serious errors. The case of pure ℓ-Se is particularly instructive, since experimentally there is a band-gap of $\sim$0.7 eV[11] under the conditions of interest, whereas our AIMD simulations show no gap, but only a deep minimum in the DOS. It is important to be clear that this does not point to any error in the DFT calculations as far as liquid structure and dynamics are concerned. What is at issue here is the (unsurprising) consequence of trying to use Kohn-Sham energies in an unjustified way. Similar large overestimates of the electronic conductivity have been reported in recent AIMD simulations on ℓ-Mg_3Bi_2[69]. However, it is not yet clear under what circumstances one should expect these large errors, and it is worth noting that the conductivity calculated in our very recent AIMD simulations on the ℓ-Ga-Se system[26] agreed quite well with experiment in spite of their low values and the existence of a deep pseudogap.

V. ATOMIC ORDERING AND ELECTRONIC PROPERTIES

We have remarked in a number of places on the ionic nature of the solid and liquid Ag-Se system, and the implications of this for understanding the structure. We now try to bring these remarks together into a coherent picture. The ionic nature of solid α-Ag_2Se is clear from an analysis of the DOS, and we have seen that the electronic structure changes little an melting, so that ℓ-Ag_2Se can be regarded as consisting approximatively of Ag^+ and Se^{2-} ions. In the more Se-rich liquid we have used the DOS and LDOS to argue that isolated Se ions are in the Se^{2-} state, while the chains consist of neutral Se atoms terminated by Se^- dangling bonds. This means that the hyperstoichiometric liquid consists of Ag^+, Se^{2-} and $(Se_n)^{2-}$ complexes. This picture can be tested by using simple charge-balance arguments to predict the average number of Se-Se bonds in the liquid at any composition, and hence the coordination number of the short distance peak in $g_{\mathrm{Se-Se}}(r)$. If the system consisted entirely of Ag^+ and Se^{2-} ions, the net charge on a system of N_{Ag} and N_{Se} ions would be $N_{\mathrm{Ag}} - 2N_{\mathrm{Se}}$. If the clusters are all $(\mathrm{Se}_n)^{2-}$ then the formation of every Se-Se bond reduces the charge by two units. For electroneutrality, the number of bonds must therefore be $N_{\mathrm{Se}} - \frac{1}{2}N_{\mathrm{Ag}}$, and the coordination number of the short distance peak in $g_{\mathrm{Se-Se}}(r)$ must be $2 - N_{\mathrm{Ag}}/N_{\mathrm{Se}} = 3 - 1/x$. This formula gives predicted values of 0, 0.62 and 1.46 for the Se-Se coordination number at the compositions $x = 0.33$, 0.42 and 0.65, which are quiet close to the values 0.1, 0.6 and 1.5 that we reported in Sec. IV B 2. This agreement confirms the picture we propose.

We can interpret the composition dependence of the experimental electrical conductivity in the light of this picture. For pure ℓ-Ag, the DOS is expected to be rather free-electron-like near E_{F}. As Se is added, electrons are drained from the Ag($5s/p$) band into the Se($4p$) states until, at the stoichiometric composition, E_{F} is in a pseudogap at the top of the Se($4p$) band. If the DOS remained rigid beyond this point, E_{F} would move into a region of higher DOS, and σ would increase strongly. Instead of this, Se-Se bonding starts to occur, and this creates a pseudogap between Se non-bonding and antibonding states. It is this that maintains σ at low values. Finally, as pure ℓ-Se is approached, this pseudogap widens, and σ falls to even lower values. As we have seen in the previous section, our numerical values of σ do not reproduce this behavior quantitatively in the hyperstoichiometric region.

If this picture is correct, it should also be rather general. It is worth noting that chalcogen pairing has been observed by diffraction experiment in some equiatomic liquid mixtures, e.g. CuSe[71] and KTe[72]. The conductivity of ℓ-Cu-Se has been measured over a range of composition and behaves in a similar way to that found in our simulations, showing a strong minimum at the composition $\mathrm{Cu_2Se}$ and then passing through a maximum in the region of CuSe before falling to the low values associated with ℓ-Se. It would clearly be interesting to investigate these and other related systems by AIMD simulation.

VI. CONCLUSIONS

The AIMD simulations we have presented lead us to the following conclusions. The reliability and realism of the DFT-pseudopotential methods we have used are demonstrated by the satisfactory predictions of the equilibrium structure of the α-$\mathrm{Ag_2Se}$ crystal a the quite close agreement with neutron diffraction results for the partial structure factors and RDFs. Nevertheless, there are significant discrepancies, which need further investigation. The simulations have shown that a large structural change in the $\mathrm{Ag}_{1-x}\mathrm{Se}_x$ liquid begins when the Se content exceeds $x = 0.33$, and this consists of the covalent bonding of Se atoms to form clusters. These clusters are mainly chain-like, but at $x = 0.65$ there is a significant fraction of three-fold coordinated Se atoms; the concentration of rings is extremely small. The equilibrium fraction of Se present in the form of clusters can be understood on a simple charge-balance argument based on an ionic interpretation. In spite of the Se clustering, the diffusion coefficients of both Ag and Se increase with Se content. This is not inconsistent with the existence of the clusters, because the Se-Se bonds turn out to have very short lifetimes of less than 1 ps. The electronic density of states of liquid $\mathrm{Ag_2Se}$ closely resembles that of the solid. With increasing Se content, the main changes in the density of states are the splitting of the Se($4s$) into bonding and anti-bonding states and the formation of Se($4p$) bonding and anti-bonding states associated with Se chains. The calculated electronic conductivity is in fair agreement with experimental values for the stoichiometric liquid, but is too large by a factor of 3 – 4 for higher Se contents. We have suggested that this error comes partly from the use of Kohn-Sham energies rather than quasiparticle energies in the conductivity calculations.

ACKNOWLEDGMENTS

The work was done within the U.K. Car-Parrinello Consortium, which is supported by the High Performance Computing Initiative. A time allocation on the Cray T3D at EPCC is acknowledged. Discussions with J. Enderby and A. Barnes, and technical help from I. Bush, M. Payne, A. Simpson and J. White played a key rôle. JMH's work is supported by EPSRC grant GR/H67935. The work used distributed hardware provided by EPSRC grants GR/H31783 and GR/J36266. Financial support from Biosym/MSI is also acknowledged.

---

[1] J. E. Enderby and A. C. Barnes, Rep. Prog. Phys. **53**, 85 (1990).
[2] F. Hensel, Adv. Phys. **28**, 555 (1979).
[3] R. W. Schmuzler, H. Hoshino, R. Fisher, and F. Hensel, Ber. Bunsenges. Phys. Chem. **80**, 107 (1976).
[4] J. E. Enderby and E. W. Collings, J. Non-Cryst. Solids **4**, 161 (1970).
[5] H. Endo, M. Yao, and K. Ishida, J. Phys. Soc. Japan **48**, 235 (1980).
[6] V. M. Glazov, S. M. Memedov, and A. S. Burkhanov, Sov. Phys.-Semicond. **20**, 263 (1986).
[7] S. Ohno, A. C. Barnes, and J. E. Enderby, J. Phys.: Condens. Matter **6**, 5335 (1994).

[8] S. Ohno, T. Okada, A. C. Barnes, and J. E. Enderby, J. Non-Cryst. Solids, at press.

[9] In detail the behavior of σ in the stoichiometric region is more complicated. There is a small peak as a function of x at x=0.33, and in a narrow region of composition σ anomalously has a negative temperature derivative (i.e. metallic)[5–8].

[10] See e. g. K. Tamura, J. Non-Cryst. Solids **117/118**, 450 (1990) and references therein.

[11] S. Hosokawa and K. Tamura, J. Non-Cryst. Solids **117/118**, 489 (1990).

[12] Y. Waseda, *Structure of Non-Crystalline Materials* (McGraw-Hill, New York, 1980).

[13] D. L. Price, M.-L. Saboungi, S. Susman, K. J. Volin, J. E. Enderby, and A. C. Barnes, J. Phys.: Condens. Matter **5**, 3087 (1993).

[14] S. B. Lague, A. C. Barnes, and P. S. Salmon, private communication.

[15] R. Bellissent and G. Tourand, J. Non-Cryst. Solids **36/36**, 1221 (1980).

[16] M. Edeling and W. Freyland, Ber. Bunsenges. Phys. Chem. **85** (1981) 1049.

[17] K. Tamura and S. Hosokawa, Ber. Bunsenges. Phys. Chem. **96** (1992) 681.

[18] D. Hohl and R. O. Jones, Phys. Rev. B **43**, (1991) 3856.

[19] F. Kirchhoff, M. J. Gillan, and J. M. Holender, J. Non-Cryst. Solids, at press.

[20] R. Car and M. Parrinello, Phys. Rev. Lett. **63**, 2471 (1985).

[21] See e.g. G. P. Srivastava and D. Weaire, Adv. Phys. **36**, 463 (1987); J. Ihm, Rep. Prog. Phys. **51**, 105 (1988); M. J. Gillan, in *Computer Simulation in Materials Science*, eds. M. Meyer and V. Pontikis, p. 257 (Kluwer, Dordrecht, 1991); G. Galli and M. Parrinello, ibid, p. 283.

[22] J. P. Rino, Y. M. M. Hornos, G. A. Antonio, I. Ebbsjö, R. K. Kalia, and P. Vashishta, J. Chem. Phys. **89**, 7542 (1988).

[23] G. Galli and M. Parrinello, J. Chem. Phys. **95**, 7504 (1991).

[24] M. Schöne, R. Kaschner, and G. Seifert, J. Phys.: Condens. Matter **7**, L19 (1995).

[25] G. A. de Wijs, G. Pastore, A. Selloni, and W. van der Lugt, Europhys. Lett. **27**, 667 (1994).

[26] J. M. Holender and M. J. Gillan, Phys. Rev. B, in press.

[27] F. Kirchhoff, J. M. Holender, and M. J. Gillan, Europhys. Lett., in press.

[28] P. Hohenberg and W. Kohn, Phys. Rev. **136**, B864 (1964).

[29] W. Kohn and L. J. Sham, Phys. Rev. **140**, A1133 (1965).

[30] R. O. Jones and O. Gunnarsson, Rev. Mod. Phys. **61**, 689 (1989).

[31] D. R. Hamann, M. Schlüter, and C. Chiang, Phys. Rev. Lett. **43**, 1494 (1979).

[32] G. B. Bachelet, D. R. Hamann, and M. Schlüter, Phys. Rev. B **26**, 4199 (1982).

[33] M. J. Gillan, J. Phys.: Condens. Matter **1**, 689 (1989).

[34] I. Štich, R. Car, and M. Parrinello, Phys. Rev. B**39**, 4997 (1989).

[35] M. C. Payne, M. P. Teter, D. C. Allan, T. A. Arias, and J. D. Joannopoulos, Rev. Mod. Phys. **64**, 1045 (1992).

[36] G. Kresse and J. Hafner, Phys. Rev. B **49**, 14251 (1994).

[37] M. P. Grumbach, D. Hohl, R. M. Martin, and R. Car, J. Phys.: Condens. Matter **6**, 1999 (1994).

[38] J. M. Holender, M. J. Gillan, M. C. Payne, and A. D. Simpson, Phys. Rev. B **52**, 967 (1995).

[39] A. Pasquarello, K. Laasonen, R. Car, C. Lee, and D. Vanderbilt, Phys. Rev. Lett. **69**, 1982 (1992).

[40] G. Kresse and J. Hafner, Phys. Rev. B **48**, 13115 (1993).

[41] L. J. Clarke, I. Štich, and M. C. Payne, Comp. Phys. Comm. **72**, 14 (1992).

[42] J.-S. Lin, A. Qteish, M. C. Payne, and V. Heine, Phys. Rev. B **47**, 4174 (1993).

[43] A. M. Rappe, K. M. Rabe, E. Kaxiras, and J. D. Joannopoulos, Phys. Rev. B **41**, 1227 (1990).

[44] G. P. Kerker, J. Phys. C **13**, L189 (1980).

[45] L. Kleinman and D. M. Bylander, Phys. Rev. Lett. **48**, 1425 (1982).

[46] R. D. King-Smith, M. C. Payne, and J. S. Lin, Phys. Rev. B **44**, 13063 (1991).

[47] F. Kirchhoff, J. M. Holender, and M. J. Gillan, Phys. Rev. B**49**, 17420 (1994).

[48] P. Rahlfs, Z. Phys. Chem. Abt. B **31**, 157 (1936).

[49] *Gmelin Handbook of Inorganic Chemistry, Silver*, edited by G. Czack, D. Koschel and H. H. Kugier (Springer Verlag, Berlin 1983), Suppl. Vol. B3, pp. 152-187.

[50] T. Sakuma, K. Iida, K. Honma, and H. Okazaki, J. Phys. Soc. Japan **43**, 538 (1977).

[51] R. J. Cava, F. Reidinger, and B. J. Wuensch, Solid State Commun. **24**, 411 (1977).

[52] R. J. Cava and D. B. McWhan, Phys. Rev. Lett. **45**, 2046 (1980).

[53] G. A. Wiegers, Amer. Mineral. **56**, 1882 (1971).

[54] A. F. Wells, *Structural Inorganic Chemistry*, 5th edition, (Clarendon Press, Oxford, 1984).

[55] R. W. G. Wyckoff, *Crystal Structures*, 2nd edition, vol. 1 (Interscience, New York, 1964).

[56] P. Engel and W. Nowacki, Acta. Cryst. B **24**, 77, (1968).

[57] L. E. Orgel, J. Chem. Soc., 4186 (1958).

[58] J. K. Burdett and O. Eisenstein, Inorg. Chem. **31**, 1758 (1992).

[59] H. J. Monkhorst and J. D. Pack, Phys. Rev. B **13**, 5188 (1976).

[60] V. M. Glazov and N. M. Makhmudova, Inorg. Materials (USSR) **6**, 1240 (1970) as reproduced in Ref.[49] p. 169.

[61] M.-L. Saboungi, W. Geertsma and D. L. Price, Annu. Rev. Phys. Chem. **41**, 207 (1990).

[62] Y. Akahama, M. Kobayashi and H. Kawamura, Phys. Rev. B**47**, 20 (1993).

[63] H. Okazaki, J. Phys. Soc. Japan **23**, 355 (1967).

[64] S. N. Mostafa, Z. Metalkde. **74**, 188 (1983).

[65] F. Kirchhoff and M. J. Gillan, unpublished.

[66] J. Robertson, Phil. Mag. B **6**, 479 (1979).

[67] N. F. Mott and E. A. Davies, *Electronic Processes in Non-Crystalline Materials*, (Clarendon, Oxford, 1979).

[68] I. Štich, R. Car, and M. Parrinello, Phys. Rev. Lett. **63**, 2240 (1989).

[69] G. A. de Wijs, PhD Thesis, University of Groningen, 1995.

[70] F. Kirchhoff, M. J. Gillan, and J. M. Holender, unpublished.

[71] A. C. Barnes and J. E. Enderby, Phil. Mag. B **58**, 497 (1988).

[72] J. Fortner, M.-L. Saboungi, and J. E. Enderby, Phys. Rev. Lett. **69**, 1415 (1992).